Canopy spectral reflectance detects oak wilt at the landscape scale using phylogenetic discrimination

Authors

Gerard Sapes[1*], Cathleen Lapadat[1], Anna K. Schweiger[1,2,3], Jennifer Juzwik[4], Rebecca Montgomery[5], Hamed Gholizadeh[6], Philip A. Townsend[7], John A. Gamon[8,9], and Jeannine Cavender-Bares[1*].

Affiliations

[1] Department of Ecology, Evolution, and Behavior, University of Minnesota, Saint Paul, Minnesota 55108, USA

[2]Institut de recherche en biologie végétale and département de sciences biologiques, Université de Montréal, Montréal, Québec, Canada

[3] Department of Geography, University of Zurich, Zurich, Switzerland

[4] Northern Research Station, USDA Forest Service, St. Paul, MN

[5] Department of Forest Resources, University of Minnesota, St. Paul, MN, 55108, USA

[6] Center for Applications of Remote Sensing, Department of Geography, Oklahoma State University, Stillwater, Oklahoma, 74078, USA

[7] Department of Forest and Wildlife Ecology, University of Wisconsin-Madison, 1630 Linden Drive, Madison, WI 53706, USA

[8]School of Natural Resources, University of Nebraska – Lincoln, Lincoln, NE, USA 68583-0961

[9] Departments of Earth & Atmospheric Sciences and Biological Sciences, University of Alberta, Edmonton, Alberta, Canada T6G 2E3

ORCID:

Gerard Sapes: https://orcid.org/0000-0002-6017-2053

Anna K. Schweiger: https://orcid.org/0000-0002-5567-4200

Hamed Gholizadeh: https://orcid.org/0000-0002-4770-7893

Philip A. Townsend: http://orcid.org/0000-0001-7003-8774

John A. Gamon: https://orcid.org/0000-0002-8269-7723

Jeannine Cavender-Bares: https://orcid.org/0000-0003-3375-9630

Author contribution statement

J.C.B. Conceived of and managed the project. G.S., C.L., A.S., J.J., R.M. and J.C.B conceived the experimental design and data analysis. C.L., A.S., and J.J. collected ground data. Z.W., H.G., P.T., and J.G. collected and processed airborne data. G.S. analyzed the data. G.S., J.C.B., and J.J., wrote the manuscript with contributions from C.L., A.S., R.M., H.G., P.T., and J.G. J.C.B, J.J., and R.M. obtained funding for this project.

Corresponding authors:

Gerard Sapes (gsapes@umn.edu) and Jeannine Cavender-Bares (cavender@umn.edu)

Phone: (406) 207-7955

Department of Ecology, Evolution, and Behavior

University of Minnesota

1987 Upper Buford Circle 55108, Saint Paul, Minnesota, USA

Abstract

The oak wilt disease caused by the invasive fungal pathogen *Bretziella fagacearum* is one of the greatest threats to oak-dominated forests across the Eastern United States. Accurate detection and monitoring over large areas are necessary for management activities to effectively mitigate and prevent the spread of oak wilt. Canopy spectral reflectance contains both phylogenetic and physiological information across the visible near-infrared (VNIR) and short-wave infrared (SWIR) ranges that can be used to identify diseased red oaks. We develop partial least square discriminant analysis (PLS-DA) models using airborne hyperspectral reflectance to detect canopies at early stages of disease development and assess the importance of VNIR, SWIR, phylogeny, and physiology for oak wilt detection. We achieve high accuracy through a three-step phylogenetic process in which we first distinguish oaks from other species (90% accuracy), then red oaks from white oaks (*Quercus macrocarpa*) (93% accuracy), and, lastly, infected from non-infected trees (80% accuracy). Including SWIR wavelengths increased model accuracy by ca. 20% relative to models based on VIS-NIR wavelengths alone; using a phylogenetic approach also increased model accuracy by ca. 20% over a single-step classification. SWIR wavelengths include spectral information important in differentiating red oaks from other species and in distinguishing diseased red oaks from healthy red oaks. We determined the most important wavelengths to identify oak species, red oaks, and diseased red oaks. We also demonstrated that several multispectral indices associated with physiological decline can detect differences between healthy and diseased trees. The wavelengths in these indices also tended to be among the most important wavelengths for disease detection within PLS-DA models, indicating a convergence of the methods. Indices were most significant for detecting oak wilt during late August, especially those associated with canopy photosynthetic activity and water status. Our study suggests that coupling phylogenetics, physiology, and canopy spectral reflectance provides an interdisciplinary and comprehensive approach that enables detection of forest diseases at large scales

even at early disease stages. These results have potential for direct application by forest managers for early detection to initiate actions to mitigate the disease and prevent pathogen spread.

Keywords: Oak wilt, photosynthetic decline, spectral reflectance, disease response, water content, remote sensing, physiology.

1. Introduction

Invasive tree pathogens are a major threat to forest diversity and function (Evans et al., 2010; Hulcr and Dunn, 2011). The damage caused by invasive species can have negative consequences for ecosystem processes and services, including air and water quality maintenance, nutrient and carbon cycling, wood and food provision, and climate regulation (Cavender-Bares et al., 2019; Díaz et al., 2019; Waller et al., 2020). In North American forests, invasive pathogens and pests that infect trees have had devastating impacts over the last century due to multiple factors, including global trade and climate change (Bergot et al., 2004; Liebhold et al., 1995; Sturrock et al., 2011), leading to the loss or potential loss of multiple foundational canopy species such as American chestnut (*Castanea dentata*), elm and ash species (*Ulmus* and *Fraxinus* spp.), and eastern hemlock (*Tsuga canadiensis*).

The oak genus (*Quercus*) is under threat from multiple pathogens and is of critical management interest due to its dominance in temperate forests of the Eastern US (Johnson et al., 2019). Oaks rank among the most diverse and important tree lineages in the United States, with 91 oak species comprising nearly 30% of biomass in US temperate forests (Cavender-Bares, 2019). Among the pathogens affecting oaks, oak wilt caused by the fungus *Bretziella fagacearum* (de Beer et al., 2017) is considered one of the most destructive threat to oaks (Appel, 1995; Haight et al., 2011; Wilson and Lindsey, 2005). The oak wilt fungus is spread below-ground from diseased trees to neighboring oaks through networks of grafted roots, thus forming centers (i.e., pockets or foci) of diseased oaks. The pathogen is also transmitted above-

ground by nitidulid beetles (family *Nitidulidae*) and oak bark beetles (*Pityophthorus spp*) (Gibbs and French 1980). Multiple species of nitidulid beetles are attracted to spore-producing fungal mats that form on branches and main stems of recently wilted red oaks (Gibbs and French, 1980; Juzwik et al., 2011; Juzwik and French, 1983). On a land parcel to larger scale, oak wilt can be most effectively controlled when newly established centers are detected and appropriately treated (Juzwik et al., 2011; Koch et al., 2010). This prevents spread or minimizes disease intensification within a stand or the surrounding landscape. Surveys of large, forested areas to identify suspect diseased trees are time-intensive and require expert training. Such surveys are needed for landscape level oak wilt management efforts. Current operational surveillance of forest landscapes in the Upper Midwest USA utilize aerial surveys conducted with fixed wing aircraft, helicopters, and UAVs (Juzwik, 2009). Other airborne imaging spectrometry offers potential for early and accurate detection of oak wilt at landscape scales.

Canopy spectral reflectance can potentially be used to detect the physiological decline resulting from oak wilt fungus infection, and thus provide forest managers with a powerful tool. Airborne spectral reflectance and indices derived from reflectance spectra have successfully been used to detect other diseases and insect damage, such as Rapid Ohia Death, Emerald Ash Borer, bark beetles, and olive decline due to *Xylella fastidiosa* (Asner et al., 2018; Lausch et al., 2013; Pontius et al., 2008, 2005; Zarco-Tejada et al., 2018). To date, spectral indices for oak wilt detection have only been developed for oak seedlings (Fallon et al., 2020). Oaks respond to oak wilt infection by forming balloon-like structures called tyloses that occlude vessels within the xylem (Juzwik and Appel, 2016; Yadeta and Thomma, Bart, 2013). Vessel occlusion potentially blocks or slows the spread of the pathogen but also reduces water transport and limits canopy physiological performance by reducing transpiration and photosynthesis and potentially causing photoinhibition (Fallon et al., 2020; Juzwik and Appel, 2016; Struckmeyer et al., 1954). In red oak species, the fungus is rapidly spread internally in the transpiration stream through large diameter springwood vessels before tylose formation limits the pathogen's spread. However, the tyloses formed

contribute to the development of wilt symptoms. Blockage of vascular conduits by tyloses and metabolites produced by the fungus can lead to declines in transpiration and canopy water content as water supply to the canopy is significantly impaired. Changes in photosynthetic activity, foliar pigment pool sizes, and water status can be detected from canopy spectra (Hanavan et al., 2015; Pontius et al., 2005; Serbin et al., 2015). Fallon et al. (2020) identified several spectral wavelengths predictive of oak wilt in greenhouse seedlings that were related to leaf photosynthesis and water status. However, spectral properties of seedlings grown and measured under greenhouse conditions may differ significantly from adult trees grown under natural conditions due to growing conditions (e.g., sun, shade, humidity, and selective filtering of solar radiation by glasshouse materials), ontogeny, canopy position, degree of canopy emergence and other factors (Cavender-Bares et al., 2020; Fernandes et al., 2020; Ollinger, 2011). Hence, it is important to explicitly test the extent to which we can detect oak wilt in natural populations of adult trees using spectral reflectance. Identification of wavelengths associated with physiological function may enable detection of trees with incipient oak wilt that would otherwise remain undetected until oak wilt damage is more extensive.

Oak lineages vary in susceptibility to oak wilt. Consequently, identification of oak subgenus is crucial to disease detection and prevention of spread. White oaks (*Quercus* subgenus *Quercus*), such as *Q. alba* and *Q. macrocarpa*, have narrower vessels (Cavender-Bares and Holbrook, 2001) and may produce tyloses efficiently (Cochard and Tyree, 1990) and in a more targeted manner in response to fungal infection (cf. Yadeta and Thomma, Bart, 2013). This slows the spread or compartmentalizes (cf. Shigo, 1984) the pathogen in infected white oak species (Jacobi and MacDonald, 1980; Koch et al., 2010; Schoenweiss, 1959). Thus, symptoms of oak wilt in white oaks appear as scattered wilt or as dieback in the crown that develops over several to many years. In contrast, red oaks (*Quercus* subgenus *Lobatae*), such as *Q. ellipsoidalis* and *Q. rubra*, have larger diameter springwood vessels and tend to delay tylose formation in response to fungal infection, limiting their effectiveness in halting the spread of the fungus through the

vascular system (Juzwik and Appel, 2016; Struckmeyer et al., 1954; Yadeta and Thomma, Bart, 2013). Thus, crown wilt symptoms in red oaks progress rapidly and lead to tree death within the same season or early in the subsequent growing season. The comparatively rapid mortality of red oaks, the common occurrence of intra-specific root grafts, and their common production of spore mats on recently wilted trees contribute to the importance of the red oak lineage in driving disease epidemics in the landscape (Menges and Loucks, 1984). Distinguishing red oaks from white oaks and other species across the landscape is therefore a critical step towards large-scale management of oak wilt. Leaf level and canopy-level modeling approaches using spectroscopic data have previously been successful in distinguishing these lineages in experimental systems and manipulated forest communities (Cavender-Bares et al., 2016; Fallon et al., 2020; Williams et al., 2020). We thus anticipate that it is possible to detect red oaks across the landscape remotely by mapping lineage identities from classification algorithms using airborne spectroscopic imagery. Here, we outline a stepwise phylogenetic approach to remote sensing of oak wilt that entails: 1) identifying trees belonging to the oak genus, 2) identifying oaks belonging to the red oak subgenus, and 3) identifying red oaks infected with oak wilt.

The goal of this study is to identify the optimal spectral range for early detection of oak wilt in red oak species (*Q. ellipsoidalis* and *Q. rubra*) across landscapes. We compare both full-range (visible, near-infrared, shortwave infrared, VSWIR, 400-2500 nm) and VNIR (visible, near-infrared, 400-1000 nm) imaging spectroscopy for accuracy of oak wilt detection. While the VNIR is sensitive to photosynthetic activity and pigments (Curran et al., 1995; Gamon and Surfus, 1999; Ustin et al., 2009), use of the SWIR provides structural and phenotypic information (Townsend et al., 2013) that is strongly coupled with phylogenetic information (Meireles et al., 2020a) including mesophyll integrity, chemical composition, and canopy water content (Jacquemoud and Ustin, 2001; Ramirez et al., 2015; Romero et al., 2012; Sims and Gamon, 2003). A second objective is to test the efficacy of spectral vegetation indices known to be sensitive to physiological decline and disease response for their ability to differentiate healthy and

diseased trees (Pontius, 2014; Pontius 2020) (Table S1). Spectral indices can increase flexibility in the detection approach because they use only a handful of wavelengths and can be easily calculated across platforms as long as the same wavelengths are present (Pontius, 2014). Spectroscopic models that require hundreds of wavelengths can have limited applicability across platforms when sensor measurement characteristics vary (Castaldi et al., 2018; Crucil et al., 2019; Nouri et al., 2017).

Here, we develop statistical models for oak wilt detection at the landscape scale using airborne spectroscopic imagery collected by two airborne systems (AISA Eagle and AVIRIS-NG) (Gholizadeh et al., 2019; Hamlin et al., 2010) covering different ranges of wavelengths (VNIR and VSWIR, respectively). We coupled on-ground tree identification and status surveys with airborne imaging spectroscopy data to assess the capacity of airborne spectroscopy to detect oak wilt during early stages of disease development in a temperate, mixed hardwood forest that included adult red oak populations. In doing so, we tested the following hypotheses:

i) Canopy reflectance from airborne spectroscopic imagery can accurately detect oak wilt infected trees in a natural forest landscape;

ii) Detection accuracy increases by first distinguishing trees in the oak genus and red oak subgenus from other species based on spectral features specific to their phylogenetic lineage;

iii) Spectral reflectance models including both VNIR and SWIR wavelengths exhibit increased accuracy relative to models including only VNIR wavelengths due to additional spectral information related to phylogenetic identity and plant structure; and

iv) Spectral indices including wavelengths associated with photosynthetic activity, pigment content, and canopy water status--associated with early symptom development in diseased red oaks--differentiate early diseased red oaks from healthy red oaks.

2. Methods

2.1 Study area

The study area was the University of Minnesota Cedar Creek Ecosystem Science Reserve (CCESR) (N 45º40'21", W 93º19'94"). Located in central Minnesota at approx. 280 m above sea level, CCESR has a continental climate with cold winters (January mean -10 °C), hot summers (July mean 22.2 °C), and a mean annual precipitation of 660 mm, spread fairly evenly throughout the year. The vegetation is comprised of a mosaic of uplands dominated by oak savanna, prairie, mixed hardwood forest, and abandoned agricultural fields, with lowlands comprised of ash and cedar swamps, acid bogs, marshes, and sedge meadows. The presence of oak wilt fungus has been documented in central Minnesota since the 1940's where it has led to widespread mortality in forests not treated for the disease. The diversity of tree species and the presence of many active oak wilt centers make CCESR well suited to assess the capacity of airborne spectroscopy to detect oak wilt in red oaks during its early stages of disease development.

2.2 Airborne data collection and tree survey

We collected two airborne imaging spectroscopy datasets across the whole study area on two dates in 2016. The first dataset was collected on 07/22/2016 between 9:08 am and 10:24 am local time using "CHAMP" (the CALMIT Hyperspectral Airborne Monitoring Platform), the University of Nebraska – Lincoln's (UNL) aircraft operated by UNL's Center for Advanced Land Management Information Technologies (CALMIT) and equipped with a pushbroom imaging spectrometer (AISA Eagle, Specim, Oulu, Finland). Data were collected at an average flight altitude of 1150 m above ground level in the northwest-southeast direction, yielding a spatial resolution of 0.75 m. The AISA Eagle comprises 488 spectral channels covering 400-982 nm with a spectral resolution of 1.25 nm and a field of view of 37.7° under nadir viewing conditions. To increase the signal-to-noise-ratio of the data, spectral on-chip binning was applied. The final product had 63 bands at ca. 9 nm intervals. The AISA Eagle images were geometrically

corrected using aircraft GPS and IMU data in Specim's CaliGeoPRO software. Radiance data were converted to reflectance using the empirical line correction (Conel et al., 1987) on reflectance measurements collected from three calibration tarps (white, grey and black, with approx. 5%, 10%, and 40% reflectance, respectively; Odyssey, Ennis Fabrics, Edmonton, Alberta, Canada) with a portable spectroradiometer (SVC HR-1024i, Spectra Vista Corporation, Poughkeepsie, NY, USA; 350 – 2500 nm) simultaneous to the overflights. SVC reflectance data were resampled to match the wavelength of airborne data and then used in the empirical line correction approach. The second dataset was collected using the Airborne Visible/Infrared Imaging Spectrometer - Next Generation (AVIRIS-NG) by the National Aeronautics and Space Administration (NASA) on 08/22/2016 starting at 03:43 PM local time at an average flight altitude of 1210 m above ground level in the near West-East direction, yielding a spatial resolution of 0.9 m. AVIRIS-NG comprises 432 spectral channels covering 380-2510 nm with a spectral resolution of 5 nm and a field of view of 36° under nadir viewing conditions. We measured the three calibration tarps with our portable spectroradiometer (SVC HR-1024i, Spectra Vista Corporation, Poughkeepsie, NY, USA; 350 – 2500 nm) during the overflights for empirical line correction. Images were delivered by the NASA Jet Propulsion Laboratory (JPL) orthorectified and preprocessed to apparent surface reflectance (Thompson et al., 2015).

About one year after collecting airborne data, between June-August of 2017, we tagged 456 adult trees of 12 species with apparently healthy crowns in woodland and savanna areas (see Table S2 for species and sample sizes) including 47 *Quercus ellipsoidalis* E.J. Hill (red oak subgenus, particularly vulnerable to oak wilt). In addition, we tagged 41 adult *Q. ellipsoidalis* trees with foliar symptoms characteristic of oak wilt (i.e., bronzing and wilting leaves in sections of the canopy) (Fig. S1). Current season crown wilt in 2017 suggested that incipient or initial crown wilt was present during mid to late August 2016 when airborne spectral data were collected. Finally, we georeferenced the canopy center of

each tagged tree using a high-precision Trimble Pro6H GPS (Trimble, Sunnyvale, CA, USA) during the leaf-off stage the following winter 2017-2018.

2.3 Canopy spectra extraction

We built a 1m-radius circular buffer around each canopy center using ArcGIS (version 10.6.1, ESRI, 2011) to sample several representative fully sunlit canopy pixels per individual tree (Table S2), which were then linked to the respective species and oak wilt status (i.e., healthy, diseased). Spectral data processing employed the package *spectrolab* (Meireles et al. 2018) in R (version 3.6.0, R Development Core Team, 2020). First, we resampled the extracted spectral data to 410-980 nm for AISA Eagle and 410-2400 nm for AVIRIS-NG (both at 5 nm resolution to match wavelengths across sensors within the VNIR range) to remove noisy wavelengths at the range ends of the sensors and reduce the number of bands in the analyses. For AVIRIS-NG data only, we removed atmospheric water absorption bands between 1335-1430 nm and 1770-1965 nm and corrected artifacts at the sensor overlap region around 950 nm. Finally, for both datasets we unit vector-normalized reflectance values to reduce illumination differences among spectra (i.e., standardize differences in amplitude) (Feilhauer et al., 2010) while preserving differences in the shape of spectra that are important for species classification (Meireles et al., 2020b). After processing spectra, we calculated 21 spectral indices commonly used in the literature related to plant photosynthetic activity (e.g., RDVI, SIPI, SIF), water status (e.g., WBI, NDWI), and photoprotective stress (e.g., PRI, CRI700, NPQI) (see Table S1 for full index list). In cases where an index required a wavelength that was not a multiple of 5 and therefore missing in our spectra, we approximated the reflectance value of that wavelength based on the reflectance of the neighboring wavelengths either by using the nearest wavelength if the difference was ≤ 1 nm or otherwise by interpolation between the two nearest wavelengths. We assessed whether vector normalization affected the capacity of spectral indexes to detect oak wilt infected trees and found no major differences in spectral index performance (Appendix S1).

238 2.4 Statistical analyses

239 All statistical analyses were performed in R (version 3.6, R Development Core Team, 2020). To
240 assess the capacity of canopy spectral reflectance to distinguish healthy trees from those infected with
241 oak wilt, we performed partial least square discriminant analyses (PLS-DAs) (Barker and Rayens, 2003)
242 using AISA Eagle (410-980 nm), AVIRIS-NG VNIR (410-980 nm), AVIRIS-NG SWIR (985-2400 nm) and AVIRIS-
243 NG VSWIR (410-2400 nm). Performing PLS-DAs for each spectral range allowed us to assess the
244 importance of each range of wavelengths for accurate detection. We treated each pixel as an observation
245 because oak wilt disease does not manifest uniformly across the canopy of a tree, especially during early
246 stages of infection. At early stages, the fungus may have infected only a fraction of the vessels within the
247 tree trunk. Thus, curtailing the water supply to a few branches that become symptomatic while others
248 remain asymptomatic. Treating pixels -rather than the whole tree- as observations is critical for early
249 detection because early infected trees may display a small number of symptomatic pixels. Thus, averaging
250 pixels across a canopy composed of mostly healthy pixels may hide the signal from the infected pixels and
251 lead to high false negative classification rates. In all PLS-DAs, we used ANOVA to compare models with
252 different numbers of components and to identify the minimal number of components that maximized
253 Kappa, a model performance statistic that quantifies model performance compared to random
254 classification (Cohen, 1960). PLS-DAs were then run with the optimal number of components and the
255 "Bayes" option to account for differences in prior probability distributions among classes (Brereton and
256 Lloyd, 2014). The optimal number of components varied by model and are reported in the results section.

257 We tested the extent to which distinguishing red oaks from other species before oak wilt status
258 classification improved the predictive performance of our models by evaluating two approaches for oak
259 wilt detection: a modelling pipeline that did not consider species identities ("direct" approach) and one
260 that differentiated red oaks from other species first ("phylogenetic" approach) (Fig. 1). Both approaches
261 were applied to each sensor type and spectral range. In the direct approach, we ignored species identities

262 and split the data within each class ("diseased" and "other") into 75:25 randomly sampled subsets for
263 model training and testing, respectively (Brereton and Lloyd, 2014; Fallon et al., 2020). We used the *caret*
264 and *pls* packages in R (Kuhn 2008, Mevik et al. 2018) to assess model performance (accuracy, sensitivity,
265 specificity, kappa) and obtain model-predicted values for each class (Congalton, 2001; Fassnacht et al.,
266 2006). The random sampling, model training, model testing, performance assessment loop was iterated
267 10,000 times to generate 10,000 different training and test subsets, classification models, and
268 corresponding performance estimates. We assessed overall performance of the direct approach by
269 calculating the average and standard deviation of the performance outputs across all iterations.

Direct Approach

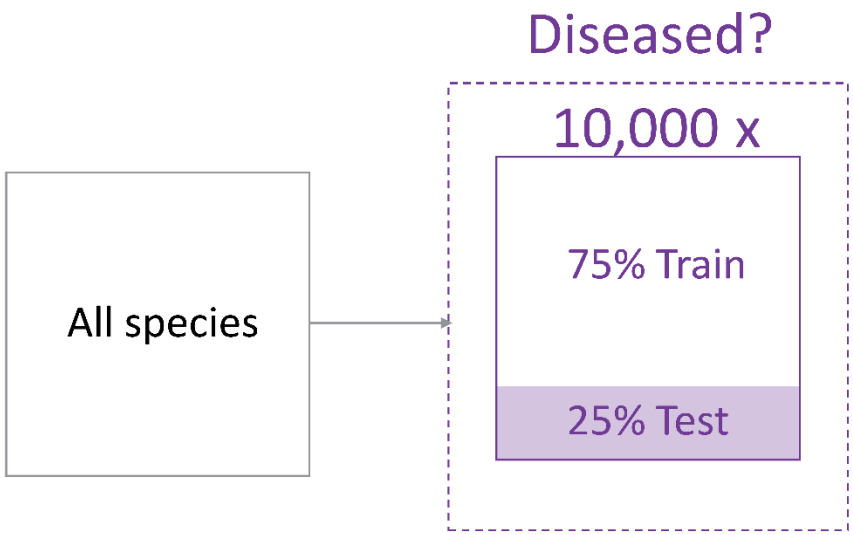

Phylogenetic Approach

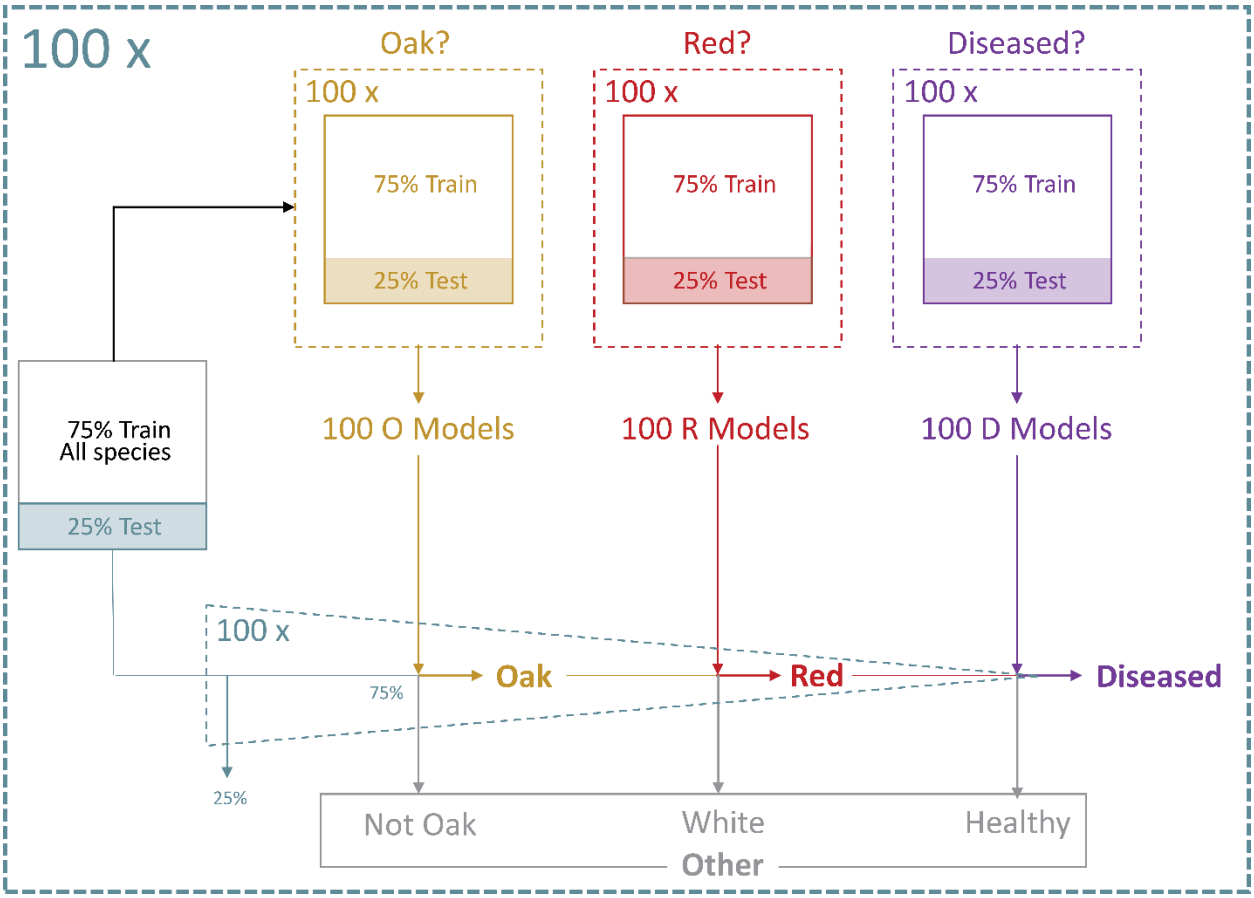

271 **Figure 1:** Workflow of the direct and phylogenetic modeling approaches used to classify diseased red oaks.
272 In the phylogenetic approach, data were randomly split into 75% and 25% for model training and testing,
273 respectively. The training set was used iteratively to train three sets of 100 models for distinguishing oaks
274 from other species, red oaks from white oaks, and diseased red oaks from healthy red oaks. The trained
275 models were coupled to filter out any observations that do not belong to the red oak group before running
276 the disease detection step. This filtering process was tested using the initial 25% withheld test data. The
277 whole process was iterated 100 times using different subsets of data to generate uncertainty around the
278 performance estimates of the model. All classification results presented in the text utilize the 25%
279 withheld data sets. See Table S3 for sample sizes within each step.

280

281 In the phylogenetic approach, we chained three distinctive PLS-DA types to solve the oak wilt
282 classification problem sequentially through the steps illustrated in Fig. 1. First, we split our data into 75:25
283 randomly sampled subsets and left the 25% aside to test the overall performance of the phylogenetic
284 approach at the end of the process (see below). Second, we used the 75% to train three types of PLS-DAs
285 specifically aimed to distinguish 1) oaks from other species, 2) red oaks from white oaks, and 3) diseased
286 red oaks from healthy red oaks. Accordingly, each model type had a different data structure: data from
287 all species for PLS-DAs that distinguished oaks from other species, data belonging to the red and white
288 oak group only for PLS-DAs that distinguished red from white oaks, and data including only putative red
289 for PLS-DAs that distinguished diseased from healthy red oaks. All three PLS-DA types were performed
290 following the same iterative approach described above by randomly sampling a subset of the 75% of the
291 data for training, testing against the unused data of the subset (a 25% of the 75%), and assessing predictive
292 performance of each PLS-DA. The purpose of these iterations was not to average model coefficients but
293 rather to test how well PLS-DA types perform on average by generating confidence intervals for model
294 performance estimates. We assessed performance of each PLS-DA type by calculating the average and

295 standard deviation of the performance estimates across all iterations. We ran a total of 100 iterations for
296 each PLS-DA type, thus obtaining 100 separate models of each type capable of distinguishing either oaks
297 from other species, red oaks from white oaks, or diseased red oaks from healthy red oaks.

298 Finally, as an independent validation, we sequentially applied the 100 models of each PLS-DA type
299 to the 25% of data originally set aside through another 100 iterations. During each iteration, the 25%
300 subset containing all species was first split into 75:25 randomly sampled subsets (stratified by class, i.e.,
301 taxonomic grouping or health status) and only the 75% of the data were used with the aim of generating
302 variation among iterations. In the first step of the phylogenetic pipeline, the selected data—which
303 included all species —were classified as either oak or "other species" using the oak discrimination model.
304 Then, the data classified as oak were classified as either "red" or "white oak" using the red oak
305 discrimination model. Lastly, the data classified as red oak were classified as either "diseased" or "healthy
306 red oak" using the disease discrimination model. Data classified as "other species", "white oak", or
307 "healthy red oak" were later reclassified as "other" and their predicted classes were compared to their
308 true identities to evaluate predictive performance. The full phylogenetic approach was iterated 100 times
309 to ensure that the initial 75% split reflected all the existing variability within the dataset. Hence, we report
310 performance across a total of 10,000 (100x100) models of each type (Fig. 1, see Table S3 for sample sizes
311 and performance). We assessed overall performance of the phylogenetic approach by calculating the
312 average and standard deviation of the multistep classification performance outputs across all iterations.
313 Additionally, we performed direct PLS-DAs to classify the 12 dominant species present in our study area
314 to identify those potentially causing misclassification of red oaks.

315 To determine which combination of wavelengths was most useful for early detection of oak wilt,
316 we extracted wavelength importance factors from PLS-DAs corresponding to AISA Eagle and AVIRIS-NG
317 VSWIR and for both direct and phylogenetic approaches using the varImp() function in *caret* (Kuhn, 2008).
318 We focused on these four PLS-DAs because they included the full range of wavelengths covered by each

sensor with and without considering species identity. For simplicity, we limited our selection to the top 20 wavelengths with the highest average importance across all iterations within each model.

To assess whether reflectance indices associated with physiology could distinguish healthy red oaks from those infected with oak wilt, we used ANOVA to perform pairwise comparisons between healthy and diseased red oaks across all spectral reflectance indices and for both AISA Eagle and AVIRIS-NG. Finally, we compared the effect sizes of these pairwise comparisons using Cohen's *d* statistic (Cohen, 1988) to assess differences in the detectability of oak wilt between late July and late August.

3. Results

All classification accuracy results are reported for the sets of 25% of samples withheld from the PLS-DA modeling steps, with the standard deviation calculated across the 10,000 iterations performed. All classification results are reported in Table S3.

3.1 Tree species classification accuracy was high

The tree species classification PLS-DA demonstrated that it is possible to accurately identify most of our 12 study species from spectral reflectance (AISA Eagle: 73.0% (±1.7%) correctly identified, AVIRIS-NG VSWIR: 89.0% (±1.3%), Appendix S2). Models correctly classified and differentiated white oaks (*Q. macrocarpa*) (AISA Eagle: 71.6% (±4.3%), AVIRIS-NG VSWIR: 87.3% (±2.2%)) and red oaks (*Q. ellipsoidalis* and *Q. rubra*) (AISA Eagle: 57.6% (±4.0%), AVIRIS-NG VSWIR: 80.4% (±2.4%)).However, models classifying the oak genus as a whole had higher accuracies (82.1% (±5.9%) and 94.0% (±5.0%) for AISA Eagle and AVIRIS-NG VSWIR, respectively, Appendix S3) than individual species models, similar to results from leaf level spectra (Cavender-Bares et al., 2016).

3.2 Spectral reflectance models detected diseased red oaks the season prior to full crown wilt

Spectral reflectance models did not accurately distinguish diseased red oaks from other trees unless red oaks were first distinguished from other species (Table S3). In the direct approach, overall model accuracy was significantly better than expected by chance (AISA Eagle: 66.2% (±6.2%), components (k) = 22; AVIRIS-NG VSWIR: 77.7% (±8.0%), k = 28, Fig. 2), but only healthy trees (true negatives) were correctly classified with high accuracy (AISA Eagle: 95.2% (±1.7%), AVIRIS-NG VSWIR: 97.8% (±1.3%), indicating high model specificity). Diseased red oaks were misclassified (false negatives) in more than 62.9% (±10.6%) and 42.5% (±14.6%) of the AISA Eagle and AVIRIS-NG VSWIR cases, respectively, indicating low model sensitivity (Fig. 2). As a result, isolating oaks and then red oaks through a stepwise phylogenetic PLS-DA model prior to disease detection reduced misclassification errors and improved the overall performance of both AISA Eagle and AVIRIS-NG VSWIR models (AISA Eagle: 83.9% (±5.9%), k = oaks: 17, red oaks: 12, diseased red oaks: 22; AVIRIS-NG VSWIR: 86% (±6.95%), k = oaks: 14, red oaks: 10, diseased red oaks: 12; Appendix S3-5, Table S3). The increase in performance was mostly due to a major increase in correct classification (true positives) of diseased red oaks (AISA Eagle: 73.9% (±9.8%), AVIRIS-NG VSWIR: 74.4% (±12.6%)) (Fig. 2, Appendix S5) resulting in increased model sensitivity compared to the direct PLS-DA approach.

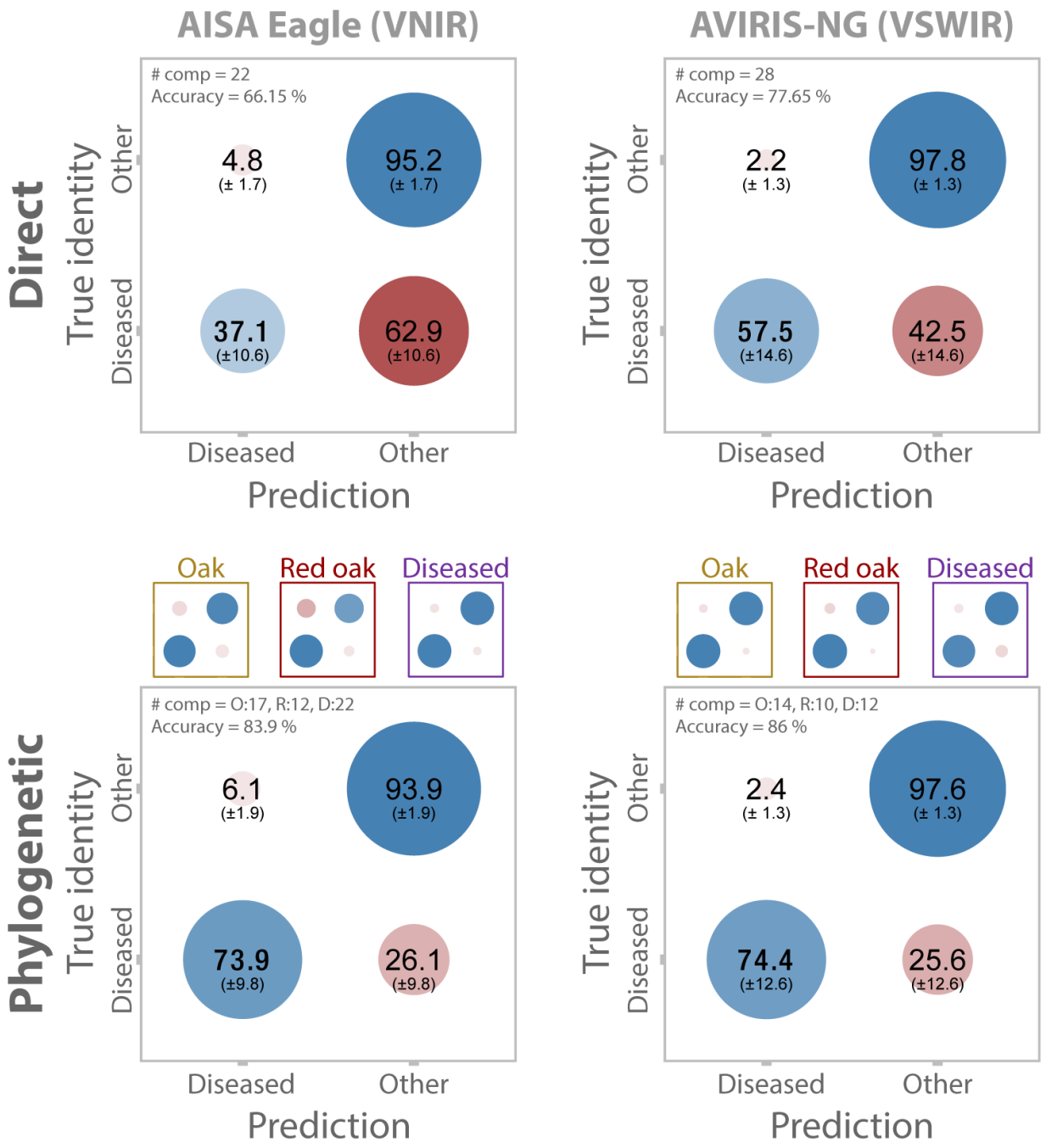

Figure 2: A stepwise phylogenetic classification approach enhanced early detection of oak wilt in red oaks. Models that included both VNIR and SWIR wavelengths (AVIRIS-NG VSWIR) showed better prediction capacity than models including VNIR only. Blue and red circles represent correct and incorrect classifications, respectively. The size and color intensity of the circle represent the average percentage of classifications into each group based on the 25% of data withheld from 10,000 model-fitting iterations,

one standard deviation is shown in parentheses. Grey boxes describe the overall predictive performance for a given approach and dataset. Red and blue circles in colored inset boxes above each phylogenetic model describe the performance of the steps within the phylogenetic model at discriminating oaks (gold), red oaks (red), and diseased red oaks (purple), respectively. The number of components used for each model or model step (O = oaks, R = red oaks, D = diseased) is given at the top left corner of the plot. See Appendices S3, S4, and S5 and Table S3 for detailed performance of the phylogenetic steps).

All steps within the phylogenetic PLS-DA model showed high performance (Table S3). The oak detection step showed high accuracy (AISA Eagle: 84% (±1.5%), k = 17; AVIRIS-NG VSWIR: 96% (±0.3%), k = 14) and only misclassified oaks as other species in 17.9% (±5.9%) and 6% (±5%) of the AISA Eagle and AVIRIS-NG VSWIR cases, respectively (Appendix S3). Similarly, the red oak detection step showed high accuracy (AISA Eagle: 85% (±2.1%), k = 12; AVIRIS-NG VSWIR: 96% (±0.6%), k = 10) and only misclassified red oaks as white oaks in 8.9% (±3.8%) and 2% (±3%) of the AISA Eagle and AVIRIS-NG VSWIR cases, respectively (Appendix S4). Finally, the diseased red oak detection step also showed high accuracy (AISA Eagle: 94% (±1.8%), k = 22; AVIRIS-NG VSWIR: 91% (±1.1%), k = 12) and misclassified diseased red oaks as healthy red oaks in only 5.5% (±1.8%) and 12.3% (±3.5%) of the AISA Eagle and AVIRIS-NG VSWIR cases, respectively (Appendix S5). We note, however, that the complexity of the model in this last step was nearly twice as high in AISA Eagle (k = 22) than in AVIRIS-NG VSWIR models (k = 12).

3.3 VNIR and SWIR ranges are both important in detecting oak wilt

AVIRIS-NG SWIR models showed slightly higher classification accuracy (true positive rate) of diseased trees than AVIRIS-NG VNIR models in both direct (AVIRIS-NG SWIR: 44.9% (±14.9%), AVIRIS-NG VNIR: 31.4% (±13.7%)) and phylogenetic approaches (AVIRIS-NG SWIR: 64.3% (±14.1%), AVIRIS-NG VNIR: 57.9% (±14.3%)) (Fig. S2). When both AVIRIS-NG VNIR and SWIR were used together, models

outperformed those using either VNIR or SWIR only. This was the case under both direct (AVIRIS-NG VSWIR: 57.5% (±14.6)) and phylogenetic approaches (AVIRIS-NG VSWIR: 74.4% (±12.6)).

When differentiating oaks from other species using AISA Eagle models, important wavelengths were clustered within the 440-550 nm, 725-750 nm, and the 850-980 nm regions of the VNIR range (Fig. 3). However, in AVIRIS-NG models that included both VNIR and SWIR, the importance of these regions was outweighed by regions 1200-1450 nm, 1600-1750 nm, and 2200-2400 nm within the SWIR range. When differentiating red oaks from white oaks using AISA Eagle models, we found important wavelengths clustered within the 700-760 nm, 780-820 nm, and 860-980 nm regions. However, in AVIRIS-NG VSWIR models, the importance of VNIR regions was strongly outweighed by regions within the SWIR range except for several wavelengths at the red-edge. Within the SWIR, the important wavelengths were clustered within 1100-1200 nm and 1490-1550 nm in addition to two spikes at 1450 nm and 1700 nm. When differentiating healthy red oaks from diseased red oaks using AISA Eagle models, important wavelengths appeared at 440 nm and across the 750-980 nm region of the VNIR range. AVIRIS-NG VSWIR models also identified important wavelengths within the 700-1000 nm range but also identified important wavelengths within the SWIR range such as wavelengths 1250, 1300, 1440, 2010, 2100, and 2320 nm. Most importantly, the twenty most important wavelengths for detection of oaks, red oaks, and diseased red oaks did not overlap in the AVIRIS-NG VSWIR models (Fig. 3). This was not the case for AISA Eagle models where several of the most important wavelengths were the same in sequential classification steps. Both AISA Eagle and AVIRIS-NG VSWIR models shared important wavelengths for oak wilt detection around 800 nm and across the 910-980 nm range.

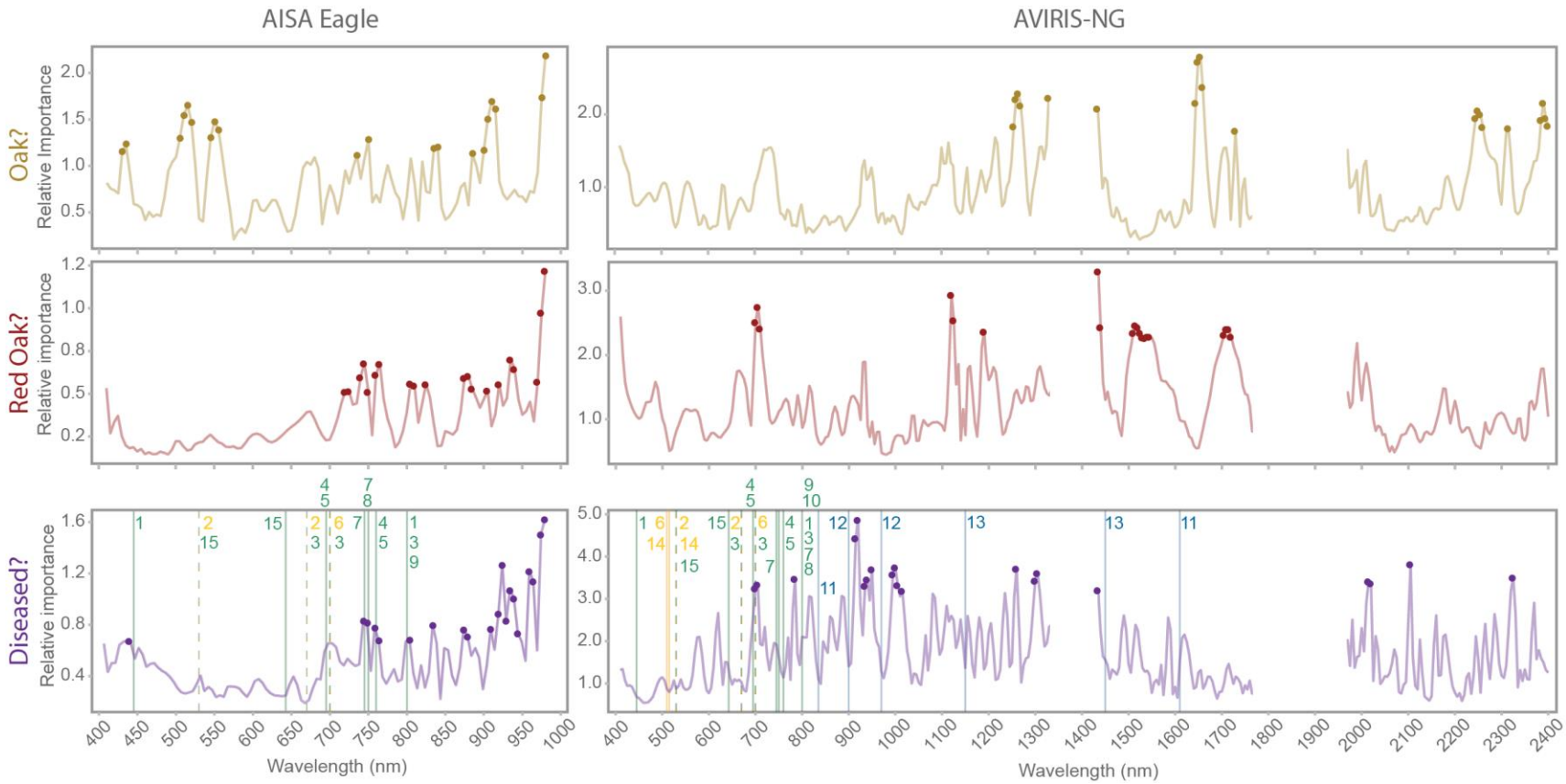

Figure 3: The twenty most important wavelengths—based on variable importance in projection (VIP)—differed among steps discriminating oaks (gold) from other species, red oaks (red) from white oaks, and diseased red oaks (purple) from healthy red oaks, and among models using either VNIR range (AISA Eagle) or both VNIR and SWIR ranges (AVIRIS-NG VSWIR). Vertical lines with numbers indicate wavelengths used in spectral indices associated with photosynthetic capacity (green), photoprotective pigment content (yellow), and water status (blue) that showed

significant differences between healthy and oak wilt-infected trees. Numbers indicate spectral indices SIPI (1), PRIM4 (2), TCARI/OSAVI (3), CMS (4), SR_{SIF} (5), CRI700 (6), VOG2 (7), CI (8), RDVI (9), SR (10), NDWI (11), WBI (12), WBI-SWIR (13), PRIm1 (14), CCI (15).

3.4 Declines in photosynthetic capacity and water status signal oak wilt

Overall, spectral indices calculated from the AVIRIS-NG dataset collected during late August showed more pronounced differences between healthy and diseased red oaks than those calculated from the AISA Eagle dataset collected in late July (Fig. 4). Spectral indices associated with canopy photosynthetic capacity showed significant differences between healthy and diseased red oaks for both sensors and time periods. Within the AISA Eagle dataset, all indices associated with photosynthetic capacity except Normalized Pigment Chlorophyll Index (NPCI) and Simple Ratio (SR) were significantly different between healthy and diseased red oaks (Table S4). Within the AVIRIS-NG dataset, all indices associated with photosynthetic capacity except NPCI were significantly different between healthy and diseased red oaks. In addition, the differences between healthy and diseased red oaks were markedly greater for AVIRIS-NG data relative to the AISA Eagle data. Most spectral indices associated with photoprotective stress showed no significant differences between healthy and diseased red oaks. Those that did—Photochemical Reflectance Index (PRIm4), Carotenoid Reflectance Index (CRI700), and (only in AVIRIS-NG) PRIm1—share wavelengths with indices of photosynthetic capacity, such as the SR and Transformed Chlorophyl Absorption in Reflectance Index/Optimized Soil-Adjusted Vegetation Index (TCARI/OSAVI) indices. Indices associated with canopy water status also showed significant differences between healthy and diseased red oaks, but only within the AVIRIS-NG dataset. The effect sizes of the differences were comparable to those of indices associated with photosynthetic capacity. Within the AISA Eagle dataset, Water Band Index (WBI)—the only spectral index associated with canopy water content

that could be calculated using the VNIR range—did not show significant differences between healthy and diseased red oaks.

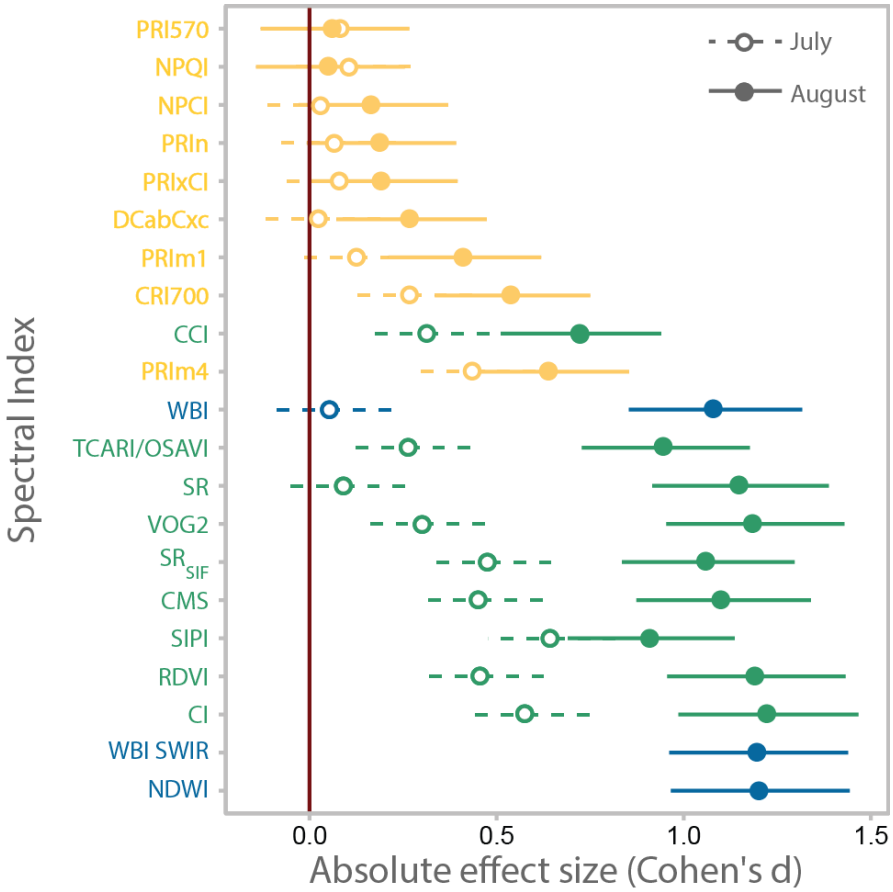

Figure 4: Spectral indices associated with photosynthetic (green) and water status (blue) differentiated early diseased red oaks from healthy red oaks. Each point represents the magnitude of the difference between healthy and diseased trees—shown by the absolute value of the Cohen's d—for a given index and time of data collection (July or August). Effect size can be understood as the amount of overlap between the distributions of two groups. For an effect size of 0, the mean of group 2 falls within the 50th percentile of group 1, and the distributions overlap completely, meaning there is no difference between them. For an effect size of 0.8, the mean of group 2 falls within the 79th percentile of group 1; thus, an average sample from group 2 would have a higher value than 79% of all samples from group 1 (Sullivan and Feinn, 2012). The Indices associated with photoprotective pigments (yellow) fail to do so

unless they also include wavelengths associated with photosynthetic capacity. Differences between healthy and diseased trees were more pronounced when indices were calculated from AVIRIS-NG spectral data collected in late August. Lines represent 95% confidence intervals. Effect sizes are significantly different from zero when their confidence intervals do not overlap with the red zero line.

4. **Discussion**

The negative impacts of oak wilt and its rate of spread across North American ecosystems calls for early detection tools that accurately identify trees affected by oak wilt at landscape scales (Haight et al., 2011; Hulcr and Dunn, 2011; Juzwik et al., 2011). We show that PLS-DA models developed from airborne spectroscopic imagery can accurately detect oak wilt-infected red oaks at early stages of disease development. We demonstrate an approach to identify oak wilt-infected red oaks, which takes advantage of the physiological and phylogenetic information embedded in their reflectance spectra (Cavender-Bares et al., 2016; Meireles et al., 2020a). By first differentiating oaks from non-oaks, and then identifying red oaks—which are highly susceptible to rapid disease development—classification models based on spectral reflectance data can be used to distinguish oak-wilt affected and healthy red oaks with high accuracy. We also found that spectral indices associated with plant photosynthesis and water status can confirm infection and are potentially sensitive to disease progression through physiological decline. Spectral indices also provide a mechanistic basis for understanding and tracking the physiological changes that allow classification models to detect oak wilt.

4.1 Including short wave infrared reflectance improves model accuracy

Including SWIR wavelengths in spectral reflectance models increases oak wilt detection accuracy. We observed higher oak wilt detectability in direct AVIRIS-NG SWIR and VSWIR than direct AISA Eagle

VNIR models. Direct PLS-DAs using AVIRIS-NG VNIR showed similar performance to that of AISA Eagle VNIR models (Fig. S2). We can therefore attribute the greater performance of direct AVIRIS-NG VSWIR models to the addition of SWIR wavelengths. Direct AISA Eagle models rely on many of the same wavelengths to distinguish red oaks from other species and to distinguish diseased and healthy red oaks (Fig. 3). As such, they often misclassify diseased red oaks as other species (Fig. 2, Appendix S3 & S4). However, even direct models show much higher accuracy when both VNIR and SWIR ranges are included (AVIRIS-NG VSWIR). The additional information-rich SWIR wavelengths allow models to use different wavelength regions to distinguish oaks from other species, red oaks from white oaks, and diseased red oaks from healthy red oaks (Fig. S2). Consequently, the critical wavelengths to identify oaks, red oaks, and diseased red oaks overlap less, which reduces the chances of confusion among classes (Fig. 3). Most likely, including SWIR reflectance provides temporally stable spectral features containing phylogenetic information associated with plant structural traits (Cavender-Bares et al., 2020; Meireles et al., 2020a) that serve to reduce misclassification of diseased red oaks as other species. Indeed, we find that the SWIR range was more important than the VNIR range in correctly identifying oak species and red oaks (Fig. 3). In particular, the 20 and 17 most important wavelengths for identifying oaks and red oaks, respectively, fell within the SWIR range. The SWIR was also important for distinguishing diseased from healthy red oaks. Among the most important SWIR wavelengths were those associated to plant water content and leaf chemistry such as protein, sugars, lignin, and cellulose content (Asner et al., 2018; Fourty et al., 1996). Based on our results, the SWIR range appears to contain disease-specific and phylogenetic information highly relevant to detecting symptoms of oak wilt and to identifying its hosts. Hence, similar to previous work combining VNIR reflectance with SIF or thermal data (Zarco-Tejada et al., 2018, 2016), when SWIR wavelengths are combined with VNIR in oak wilt detection models, detection rates are maximized.

4.2 A multi-step phylogenetic approach increases accuracy

Partitioning the classification process into simple binary steps within a phylogenetic framework reduces potential misclassification and increases model accuracy. We used a hierarchical classification approach (Allen and Walsh, 1996; Townsend et al., 2009; Wolter et al., 1995) aimed towards distinguishing the more susceptible red oaks from white oaks and other species that are less susceptible to oak wilt. During the first step, phylogenetic models distinguish between oaks and other species because the reflectance spectrum shows phylogenetic conservatism among the oaks (Cavender-Bares et al., 2016; Cavender-Bares, 2019), including those infected by oak wilt. The model is not required to distinguish between healthy and diseased conspecifics in this first step, thus simplifying the task. Reducing the number of potential classes becomes increasingly important as the individuals become more phylogenetically related—and hence more phenotypically similar—which makes correct classification more challenging (Meireles et al., 2020b). Removing non-oak species significantly reduces variation in phylogenetically conserved regions of the spectra, allowing the model to be trained on spectral differences that distinguish white and red oaks and subsequently on the spectral variation that distinguishes diseased and healthy red oaks. Because of these filtering steps, the disease detection algorithm is highly accurate (>90%; Fig. 2, appendix S5) and significantly more accurate than a single-step, direct approach. While the phylogenetic approach gains complexity in terms of number of steps, each binary classification step is simple and requires few independent components. Although each step generates classification errors that propagate through the modeling pipeline, these errors are captured by the overall performance metrics, indicating that the increase in accuracy gained through the phylogenetic filtering outweighs the propagated errors. Interestingly, implementing a stepwise phylogenetic approach boosted model performance to a greater extent in AISA Eagle and AVIRIS-NG VNIR than in AVIRIS-NG VSWIR models. This suggests that the main contribution of the phylogenetic approach is the same as that of adding SWIR range. The phylogenetic approach increases accuracy by reducing the number of classes to compare while inclusion of the SWIR range increases accuracy by increasing the

514 number of informative wavelengths. Reduced boosts from using the stepwise phylogenetic approach in
515 the performance in AVIRIS-NG VSWIR relative to VNIR models may be a consequence of including SWIR
516 and increasing informative wavelengths beyond what is available within the VNIR, avoiding
517 misclassification (see previous section, Fig. 3). Reduced boosts in AVIRIS-NG VNIR relative to AISA Eagle
518 VNIR models could be due to differences in sampling date or to sensor type and/or data quality (e.g.,
519 associated with spectral binning and/or signal-to-noise).

520 Our results highlight that species classification is critical for increasing model accuracy for a simple
521 reason: if the disease is host-specific, modeling can be more tractable by detecting potential hosts first.
522 Future studies should test whether phylogenetic models with simple binary classification steps such as
523 the one used here make disease detection models generic enough to be applicable across different sites
524 and years.

525 *4.3 Targeted spectral indices help understand physiological changes associated with oak wilt disease*

526 Diseased red oaks were more easily differentiated from healthy red oaks by spectral reflectance
527 indices associated with photosynthetic activity (Carter and Knapp, 2001; Vogelmann et al., 1993; Zarco-
528 Tejada et al., 2002) and water status (Ceccato et al., 2001; Serrano et al., 2000; Ullah et al., 2014) than by
529 photoprotective pigment content indices. Indices based on photoprotective pigment content could not
530 differentiate diseased trees from asymptomatic trees unless they included wavelengths also associated
531 with photosynthetic activity (Figs. 3 & 4). These results suggest that oak wilt infection in adult trees in
532 natural ecosystems triggers declines in photosynthetic rate, stomatal conductance, and water content
533 just as in greenhouse seedlings (Fallon et al., 2020). All indices showed greater sensitivity in late August
534 relative to late July suggesting that oak wilt symptoms had progressed. Moreover, our results also uncover
535 an important temporal pattern in physiological decline: photosynthesis declines first, and dehydration
536 follows. By July, indices of photosynthetic activity showed greater sensitivity to oak wilt than indices of

537 water status (Fig. 4). At early stages, both tylose production (in response to infection) and plugging of
538 vessels by metabolites of the fungus are likely to have contributed to diminished water transport. In turn,
539 reduced transpiration and stomatal closure induced by reduced water supply is expected to have caused
540 photosynthetic decline (Fallon et al., 2020). However, trees may not yet have experienced enough
541 vascular occlusion to cause canopy dehydration. By August, water status indices showed greater overall
542 sensitivity to oak wilt than photosynthetic activity indices (Fig. 4). Although different sensors were used
543 at each time point, the normalized indices should be comparable across sensor types. The results are
544 consistent with experimental work indicating that photosynthesis is the first physiological process to
545 decline as stomata shut down (Fallon et al., 2020) followed by water content as vessel occlusion develops
546 and the fungus damages cell walls and membranes (e.g., through pathogen-produced toxins) leading to
547 dehydration and tissue death (Oliva et al., 2014). Pairing photosynthetic activity and water status indices
548 can provide powerful tools to delineate oak wilt centers across areas of the landscape dominated by red
549 oaks. Pockets of affected trees may show a center-outward radial gradient with dry dead trees at the
550 center, dehydrated and photosynthetically impaired trees in the middle, and trees with slightly lower
551 photosynthetic capacity than expected around the edge of the pocket (i.e., early disease development
552 phase) (Figs. 5, S3, & S4). Hence, paired indices could provide information about the stage of disease
553 development, thus allowing managers to better assess risk of spread and adjust the magnitude of their
554 interventions accordingly (Pontius and Hallett, 2014).

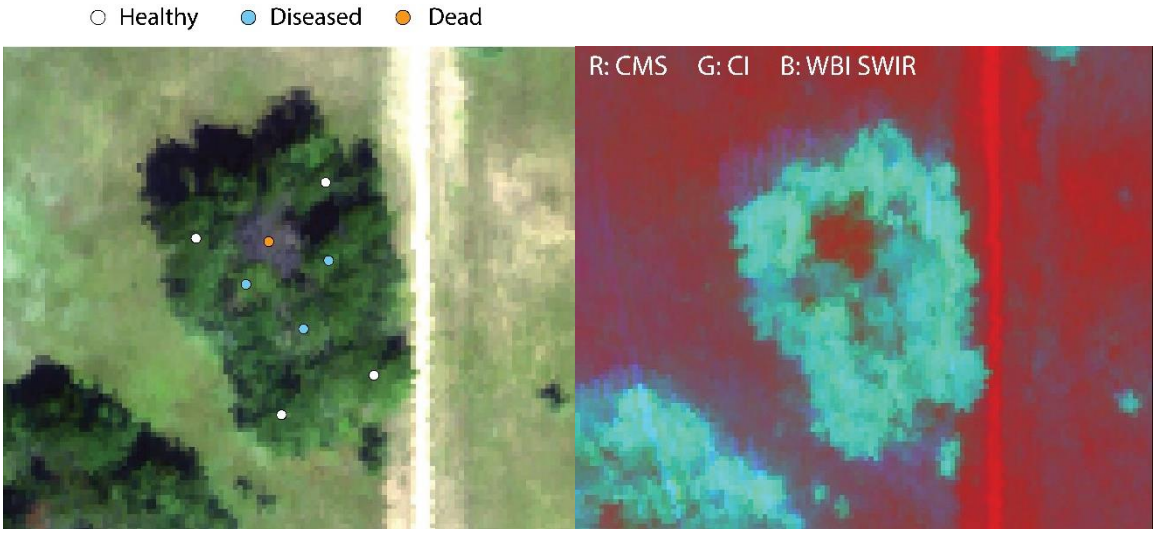

Figure 5. A typical oak wilt pocket observed through true color and a combination of spectral indices using the 2016 AVIRIS-NG data. A tree killed by oak wilt during 2015 (orange circle) can be observed at the center of the oak wilt pocket in true color (red as 640 nm, green as 550 nm, and blue as 470 nm). Three diseased trees (blue circles) stand next to it that cannot be detected with true color images. Both dead and diseased trees are surrounded by an outer ring of healthy trees. Diseased trees become apparent through spectral indices associated with photosynthetic function and water status -such as the Carter-Miller Stress index (CMS), Chlorophyll Index red edge (CI), and Water Band Index in the SWIR range (WBI SWIR)- placed on the red (R), green (G), and blue (B) channels.

5. Conclusions

Protecting ecosystems from the threats of invasive species resulting from globalization and a changing climate is one of the most pressing challenges of our times (Díaz et al., 2019; Liebhold et al., 1995; Waller et al., 2020). Early detection greatly enhances the ability of managers to prevent the

enormous ecological and economical damage caused by invasive species (Juzwik, 2000; Poland et al., 2021). Airborne spectroscopic imagery enables landscape-level detection of diseases caused by invasive pathogens, like oak wilt, at their earliest stages due to the phylogenetic and physiological information embedded in spectral reflectance. SWIR wavelengths increased model accuracy by enabling detection of disease-specific hosts, a critical step in identifying forested areas vulnerable to infection. Additionally, inference of the physiological basis of oak wilt symptom development using spectral indices associated with known spectral features points to the potential to delineate oak wilt centers using remote sensing products that monitor canopy photosynthetic capacity and water status. Importantly, in our study landscape detection was made possible by coupling airborne spectroscopic imagery with traditional knowledge from taxonomic and disease experts and high precision ground GPS reference data. While landscape detection of oak wilt will facilitate the task of detecting infected trees, there is still much work to do. Future studies should assess whether PLS-DA models will be general enough to detect oak wilt across years and sites and whether the physiological basis of oak wilt symptom development will be sufficient to make accurate inferences about the presence of new oak wilt infections. Further investigation of the physiological changes that accompany disease progression may also provide the link to scale spectral detection to regional scales via spaceborne platforms. The work done here points to the benefit of research that might lead to an “optimal” remote sensing system (airborne or satellite) for detecting invasive diseases. We hope that our research motivates such work.

Acknowledgements

This project was funded by the Minnesota Invasive Terrestrial Plants and Pests Center, the National Science Foundation (NSF) and the National Aeronautics and Space Administration (NASA) through the Dimensions of Biodiversity program (DEB-1342872 and DEB-1342778), the Cedar Creek Long Term Ecological Research program (1831944), and the NSF Biology Integration Institute ASCEND (DBI: 2021898).

The University of Minnesota, including Cedar Creek ESR, lies on the ancestral, traditional, and contemporary Land of the Dakota people. We would like to thank Brett Fredericksen, Erin Murdock, Kali Hall, Lewis French and Travis Cobb for help with tarp measurement for empirical line corrections. Thanks to Dr. Joe Knight for access to the infrastructure of the Remote Sensing and Geospatial Analysis Lab at UMN, and to Dan Bahauddin for informatics help which facilitated flight planning at Cedar Creek. We thank Paul Castillo, USFS for his technical assistance in the training of field technicians, and Zhihui Wang for assistance processing AVIRIS-NG imagery. We also thank Shan Kothari, Lucy Shroeder, Anna Yang, Austin Yantes, Clarissa Fontes, Byju Govidan, Artur Stefanski, and Adriana Castillo Castillo for their comments in previous versions of this manuscript.

References

Allen, T.R., Walsh, S.J., 1996. Spatial and compositional pattern of alpine treeline, Glacier National Park, Montana. Photogramm. Eng. Remote Sensing 62, 1261–1268.

Appel, D.N., 1995. The Oak Wilt Enigma: Perspectives from the Texas Epidemic. Annu. Rev. Phytopathol. 33, 103–118. https://doi.org/10.1146/annurev.py.33.090195.000535

Asner, P., Martin, R.E., Keith, L.M., Heller, W.P., Hughes, M.A., Vaughn, R., Hughes, R.F., Balzotti, C., 2018. A Spectral Mapping Signature for the Rapid Ohia Death (ROD) Pathogen in Hawaiian Forests. Remote Sens. 10, 1–14. https://doi.org/10.3390/rs10030404

Barker, M., Rayens, W., 2003. Partial least squares for discrimination. J. Chemom. https://doi.org/10.1002/cem.785

Bergot, M., Cloppet, E., Pérarnaud, V., Déqué, M., Marçais, B., Desprez-Loustau, M.-L., 2004. Simulation of potential range expansion of oak disease caused by Phytophthora cinnamomi under climate

change. Glob. Chang. Biol. 10, 1539–1552. https://doi.org/10.1111/j.1365-2486.2004.00824.x

Brereton, R.G., Lloyd, G.R., 2014. Partial least squares discriminant analysis: Taking the magic away. J. Chemom. 28, 213–225. https://doi.org/10.1002/cem.2609

Carter, G.A., Knapp, A.K., 2001. Leaf optical properties in higher plants: linking spectral characteristics to stress and chlorophyll concentration. Am. J. Bot. https://doi.org/10.2307/2657068

Castaldi, F., Chabrillat, S., Jones, A., Vreys, K., Bomans, B., Wesemael, B. Van, 2018. Soil Organic Carbon Estimation in Croplands by Hyperspectral Remote APEX Data Using the LUCAS Topsoil Database. Remote Sens. 10, 2–19. https://doi.org/10.3390/rs10020153

Cavender-Bares, J., Gamon, J.A., Townsend, P.A. (Eds.), 2020. Remote Sensing of Plant Biodiversity, Remote Sensing of Plant Biodiversity. Springer International Publishing, Cham. https://doi.org/10.1007/978-3-030-33157-3

Cavender-Bares, J., Holbrook, N.M., 2001. Hydraulic properties and freezing-induced cavitation in sympatric evergreen and deciduous oaks with contrasting habitats. Plant. Cell Environ. 24, 1243–1256. https://doi.org/10.1046/j.1365-3040.2001.00797.x

Cavender-Bares, J., Meireles, J.E., Couture, J.J., Kaproth, M.A., Kingdon, C.C., Singh, A., Serbin, S.P., Center, A., Zuniga, E., Pilz, G., Townsend, P.A., 2016. Associations of leaf spectra with genetic and phylogenetic variation in oaks: Prospects for remote detection of biodiversity. Remote Sens. 221, 1–17. https://doi.org/10.3390/rs8030221

Cavender-Bares, J., Nelson, E., Meireles, J.E., Lasky, J., Miteva, D., Nowak, D., Pearse, W., Helmus, M., Zanne, A., Fagan, W., Mihiar, C., Muller, N., Kraft, N., Polasky, S., 2019. The hidden value of trees: quantifying the ecosystem services of tree lineages and their major threats across the continental US. EcoEvorxiv Prepr. 1–42. https://doi.org/10.32942/osf.io/gp7mt

Cavender-Bares, J., 2019. Diversification, adaptation, and community assembly of the American oaks (Quercus), a model clade for integrating ecology and evolution. New Phytol. 221, 669–692. https://doi.org/10.1111/nph.15450

Ceccato, P., Flasse, S., Tarantola, S., Jacquemoud, S., Grégoire, J.M., 2001. Detecting vegetation leaf water content using reflectance in the optical domain. Remote Sens. Environ. 77, 22–33. https://doi.org/10.1016/S0034-4257(01)00191-2

Cochard, H., Tyree, M.T., 1990. Xylem dysfunction in Quercus: vessel sizes, tyloses, cavitation and seasonal changes in embolism. Tree Physiol. 6, 393–407. https://doi.org/10.1093/treephys/6.4.393

Cohen, J., 1988. The effect size index: d, in: Statistical Power Analysis for the Behavioral Sciences.

Conel, J.E., Green, R.O., Vane, G., Bruegge, C.J., Alley, R.E., Curtiss, B.J., 1987. AIS-2 Radiometry and a Comparison of Methods for the Recovery of Ground Reflectance, in: Third Airborne Imaging Spectrometer Data Analysis Workshop. Jet Propulsion Lab, Pasadena, CA, pp. 18–47.

Congalton, R.G., 2001. Accuracy assessment and validation of remotely sensed and other spatial information. Int. J. Wildl. Fire 10, 321. https://doi.org/10.1071/WF01031

Crucil, G., Castaldi, F., Aldana-jague, E., Wesemael, B. Van, Macdonald, A., Van Oost, K., 2019. Assessing the Performance of UAS-Compatible Multispectral and Hyperspectral Sensors for Soil Organic Carbon Prediction. Sustainability 11, 2–18. https://doi.org/10.3390/su11071889

Curran, P.J., Windham, W.R., Gholz, H.L., 1995. Exploring the relationship between reflectance red edge and chlorophyll concentration in slash pine leaves. Tree Physiol. 15, 203–206. https://doi.org/10.1093/treephys/15.3.203

de Beer, Z.W., Marincowitz, S., Duong, T.A., Wingfield, M.J., 2017. Bretziella, a new genus to accommodate the oak wilt fungus, Ceratocystis fagacearum (Microascales, Ascomycota). MycoKeys

27, 1–19. https://doi.org/10.3897/mycokeys.27.20657

Díaz, S., Settele, J., Brondízio, E.S., Ngo, H.T., Agard, J., Arneth, A., Balvanera, P., Brauman, K.A., Butchart, S.H.M., Chan, K.M.A., Garibaldi, L.A., Ichii, K., Liu, J., Subramanian, S.M., Midgley, G.F., Miloslavich, P., Molnár, Z., Obura, D., Pfaff, A., Polasky, S., Purvis, A., Razzaque, J., Reyers, B., Chowdhury, R.R., Shin, Y.-J., Visseren-Hamakers, I., Willis, K.J., Zayas, C.N., 2019. Pervasive human-driven decline of life on Earth points to the need for transformative change. Science (80-.). 366, eaax3100. https://doi.org/10.1126/science.aax3100

ESRI, 2011. ArcGIS Desktop: Release 10. Redlands, CA: Environmental Systems Research Institute. Redlands.

Evans, E.A., Crane, J., Hodges, A., Osborne, J.L., 2010. Potential economic impact of laurel wilt disease on the Florida avocado industry. Horttechnology 20, 234–238. https://doi.org/10.21273/horttech.20.1.234

Fallon, B., Yang, A., Lapadat, C., Armour, I., Juzwik, J., Montgomery, R.A., Cavender-bares, J., 2020. Spectral differentiation of oak wilt from foliar fungal disease and drought is correlated with physiological changes. Tree Physiol. 40, 377–390. https://doi.org/10.1093/treephys/tpaa005

Fassnacht, K.S., Cohen, W.B., Spies, T.A., 2006. Key issues in making and using satellite-based maps in ecology: A primer. For. Ecol. Manage. https://doi.org/10.1016/j.foreco.2005.09.026

Feilhauer, H., Asner, G.P., Martin, R.E., Schmidtlein, S., 2010. Brightness-normalized Partial Least Squares Regression for hyperspectral data. J. Quant. Spectrosc. Radiat. Transf. 111, 1947–1957. https://doi.org/10.1016/j.jqsrt.2010.03.007

Fernandes, A.M., Fortini, E.A., Müller, L.A. de C., Batista, D.S., Vieira, L.M., Silva, P.O., Amaral, C.H. do, Poethig, R.S., Otoni, W.C., 2020. Leaf development stages and ontogenetic changes in passionfruit

(Passiflora edulis Sims.) are detected by narrowband spectral signal. J. Photochem. Photobiol. B Biol. https://doi.org/10.1016/j.jphotobiol.2020.111931

Fourty, T., Baret, F., Jacquemoud, S., Schmuck, G., Verdebout, J., 1996. Leaf optical properties with explicit description of its biochemical composition: Direct and inverse problems. Remote Sens. Environ. 56, 104–117. https://doi.org/10.1016/0034-4257(95)00234-0

Gamon, J.A., Surfus, J.S., 1999. Assessing leaf pigment content and activity with a reflectometer. New Phytol. 143, 105–117. https://doi.org/10.1046/j.1469-8137.1999.00424.x

Gholizadeh, H., Gamon, J.A., Townsend, P.A., Zygielbaum, A.I., Helzer, C.J., Hmimina, G.Y., Yu, R., Moore, R.M., Schweiger, A.K., Cavender-Bares, J., 2019. Detecting prairie biodiversity with airborne remote sensing. Remote Sens. Environ. 221, 38–49. https://doi.org/10.1016/j.rse.2018.10.037

Gibbs, J.N., French, D.W., 1980. The transmission of oak wilt, USDA Forest Service, North Central Research Station.

Haight, R.G., Homans, F.R., Horie, T., Mehta, S. V., Smith, D.J., Venette, R.C., 2011. Assessing the Cost of an Invasive Forest Pathogen: A Case Study with Oak Wilt. Environ. Manage. 47, 506–517. https://doi.org/10.1007/s00267-011-9624-5

Hamlin, L., Green, R.O., Mouroulis, P., Eastwood, M., Mccubbin, I., Wilson, D., Randall, D., Dudik, M., 2010. Imaging Spectrometer Science Measurements for Terrestrial Ecology : AVIRIS and the Next Generation AVIRIS Characteristics and Development Status, in: NASA Earth Science Technology Forum. pp. 1–7.

Hanavan, R.P., Pontius, J., Hallett, R., 2015. A 10-Year Assessment of Hemlock Decline in the Catskill Mountain Region of New York State Using Hyperspectral Remote Sensing Techniques. J. Econ. Entomol. 1–11. https://doi.org/10.1093/jee/tou015

Hulcr, J., Dunn, R.R., 2011. The sudden emergence of pathogenicity in insect–fungus symbioses threatens naive forest ecosystems. Proc. R. Soc. B Biol. Sci. 278, 2866–2873. https://doi.org/10.1098/rspb.2011.1130

Jacobi, W., MacDonald, W., 1980. Colonization of Resistant and Suceptible Oaks by Ceratocystis Fagacearum. Phytopathology 70, 618–623.

Jacquemoud, S., Ustin, S.L., 2001. Leaf optical properties: a state of the art. Proc. 8th Int. Symp. Phys. Meas. Signatures Remote Sens. https://doi.org/10.1017/CBO9781107415324.004

Johnson, P.S., Shifley, S.R., Rogers, R., 2019. The ecology and silviculture of oaks, The ecology and silviculture of oaks. CABI, Wallingford. https://doi.org/10.1079/9781780647081.0000

Juzwik, J., 2009. Epidemiology and occurrence of oak wilt in Midwestern, middle, and south Atlantic states., in: Proceedings of the National Oak Wilt Symposium. Texas Forest Service Publication, Austin, TX, pp. 49–60.

Juzwik, J., 2000. An oak wilt primer. Int. Oaks 11, 14–20.

Juzwik, J., Appel, D.N., 2016. Diseases of trees in the Great Plains: Oak Wilt, in: Diseases of Trees in the Great Plains. USDA, Forest Service, Rocky Mountain Forest and Range Station, Fort Collins, Colo. :, pp. 129–133. https://doi.org/Gen. Tech. Rep. RMRS-GTR-335

Juzwik, J., Appel, D.N., MacDonald, W.L., Burks, S., 2011. Challenges and Successes in Managing Oak Wilt in the United States. Plant Dis. 95, 888–900. https://doi.org/10.1094/PDIS-12-10-0944

Juzwik, J., French, D.W., 1983. Ceratocystis fagacearum and C. piceae on the Surfaces of Free-Flying and Fungus-Mat-Inhabiting Nitidulids. Phytopathology 73, 1164–1168. https://doi.org/10.1094/phyto-73-1164

Koch, K.A., Quiram, G.L., Venette, R.C., 2010. A review of oak wilt management: A summary of treatment options and their efficacy. Urban For. Urban Green. 9, 1–8. https://doi.org/10.1016/j.ufug.2009.11.004

Kuhn, M., 2008. Building Predictive Models in R Using the caret Package. J. Stat. Softw. 28. https://doi.org/10.18637/jss.v028.i05

Lausch, A., Heurich, M., Gordalla, D., Dobner, H.J., Gwillym-Margianto, S., Salbach, C., 2013. Forecasting potential bark beetle outbreaks based on spruce forest vitality using hyperspectral remote-sensing techniques at different scales. For. Ecol. Manage. 308, 76–89. https://doi.org/10.1016/j.foreco.2013.07.043

Liebhold, A.M., MacDonald, W.L., Bergdahl, D., Mastro, V.C., 1995. Invasion by Exotic Forest Pests: A Threat to Forest Ecosystems. For. Sci. 41, a0001-z0001. https://doi.org/10.1093/forestscience/41.s1.a0001

Meireles, J.E., Cavender-Bares, J., Townsend, P.A., Ustin, S., Gamon, J.A., Schweiger, A.K., Schaepman, M.E., Asner, G.P., Martin, R.E., Singh, A., Schrodt, F., Chlus, A., O'Meara, B.C., 2020a. Leaf reflectance spectra capture the evolutionary history of seed plants. New Phytol. nph.16771. https://doi.org/10.1111/nph.16771

Meireles, J.E., O'Meara, B., Cavender-Bares, J., 2020b. Linking Leaf Spectra to the Plant Tree of Life, in: Remote Sensing of Plant Biodiversity. Springer International Publishing, Cham, pp. 155–172. https://doi.org/10.1007/978-3-030-33157-3_7

Menges, E.S., Loucks, O.L., 1984. Modeling a Disease-Caused Patch Disturbance: Oak Wilt in the Midwestern United States. Ecology 65, 487–498. https://doi.org/10.2307/1941411

Nouri, M., Gomez, C., Gorretta, N., Roger, J.M., 2017. Clay content mapping from airborne hyperspectral

Vis-NIR data by transferring a laboratory regression model. Geoderma 298, 54–66. https://doi.org/10.1016/j.geoderma.2017.03.011

Oliva, J., Stenlid, J., Martinez-Vilalta, J., 2014. The effect of fungal pathogens on the water and carbon economy of trees: implications for drought-induced mortality. New Phytol. 203, 1028–1035.

Ollinger, S. V., 2011. Sources of variability in canopy reflectance and the convergent properties of plants. New Phytol. 189, 375–394. https://doi.org/10.1111/j.1469-8137.2010.03536.x

Poland, T.M., Patel-Weynand, T., Finch, D., Fort Miniat, C., Hayes, D.C., Lopez, V., 2021. Invasive Species in Forests and Grasslands of the United States: A Comprehensive Science Synthesis for the United States Forest Sector. Springer Verlag, Cham, Switzerland.

Pontius, J., 2014. A new approach for forest decline assessments: Maximizing detail and accuracy with multispectral imagery. Int. J. Remote Sens. 35, 3384–3402. https://doi.org/10.1080/01431161.2014.903439

Pontius, J., Hallett, R., 2014. Comprehensive methods for earlier detection and monitoring of forest decline. For. Sci. https://doi.org/10.5849/forsci.13-121

Pontius, J., Hallett, R., Martin, M., 2005. Using AVIRIS to assess hemlock abundance and early decline in the Catskills, New York. Remote Sens. Environ. 97, 163–173. https://doi.org/10.1016/j.rse.2005.04.011

Pontius, J., Martin, M., Plourde, L., Hallett, R., 2008. Ash decline assessment in emerald ash borer-infested regions : A test of tree-level, hyperspectral technologies. Remote Sens. Environ. 112, 2665–2676. https://doi.org/10.1016/j.rse.2007.12.011

R Development Core Team, 2020. R: A Language and Environment for Statistical Computing. version 3.6.0.

Ramirez, J.A., Posada, J.M., Handa, I.T., Hoch, G., Vohland, M., Messier, C., Reu, B., 2015. Near-infrared spectroscopy (NIRS) predicts non-structural carbohydrate concentrations in different tissue types of a broad range of tree species. Methods Ecol. Evol. 6, 1018–1025. https://doi.org/10.1111/2041-210X.12391

Romero, A., Aguado, I., Yebra, M., 2012. Estimation of dry matter content in leaves using normalized indexes and prospect model inversion. Int. J. Remote Sens. 33, 396–414. https://doi.org/10.1080/01431161.2010.532819

Schoenweiss, D.F., 1959. Xylem formation as a factor in oak wilt resistance. Phytopathology 49, 335–337.

Serbin, S.P., Singh, A., Desai, A.R., Dubois, S.G., Jablonski, A.D., Kingdon, C.C., Kruger, E.L., Townsend, P.A., 2015. Remotely estimating photosynthetic capacity, and its response to temperature, in vegetation canopies using imaging spectroscopy. Remote Sens. Environ. 167, 78–87. https://doi.org/10.1016/j.rse.2015.05.024

Serrano, L., Ustin, S.L., Roberts, D.A., Gamon, J.A., Peñuelas, J., 2000. Deriving water content of chaparral vegetation from AVIRIS data. Remote Sens. Environ. https://doi.org/10.1016/S0034-4257(00)00147-4

Shigo, A.L., 1984. Compartmentalization: A Conceptual Framework for Understanding How Trees Grow and Defend Themselves. Annu. Rev. Phytopathol. 22, 189–214. https://doi.org/10.1146/annurev.py.22.090184.001201

Sims, D.A., Gamon, J.A., 2003. Estimation of vegetation water content and photosynthetic tissue area from spectral reflectance: A comparison of indices based on liquid water and chlorophyll absorption features. Remote Sens. Environ. https://doi.org/10.1016/S0034-4257(02)00151-7

Struckmeyer, B.E., Beckman, C.H., Kuntz, J.E., Riker, A.J., 1954. Plugging of vessels by tyloses and gums in wilting oaks. Phytopathology 44, 148–153.

Sturrock, R.N., Frankel, S.J., Brown, A. V., Hennon, P.E., Kliejunas, J.T., Lewis, K.J., Worrall, J.J., Woods, A.J., 2011. Climate change and forest diseases. Plant Pathol. 60, 133–149. https://doi.org/10.1111/j.1365-3059.2010.02406.x

Sullivan, G.M., Feinn, R., 2012. Using Effect Size—or Why the P Value Is Not Enough. J. Grad. Med. Educ. 4, 279–282. https://doi.org/10.4300/JGME-D-12-00156.1

Thompson, D.R., Gao, B., Green, R.O., Roberts, D.A., Dennison, P.E., Lundeen, S.R., 2015. Atmospheric correction for global mapping spectroscopy: ATREM advances for the HyspIRI preparatory campaign. Remote Sens. Environ. 167, 64–77. https://doi.org/10.1016/j.rse.2015.02.010

Townsend, P.A., Helmers, D.P., Kingdon, C.C., McNeil, B.E., de Beurs, K.M., Eshleman, K.N., 2009. Changes in the extent of surface mining and reclamation in the Central Appalachians detected using a 1976–2006 Landsat time series. Remote Sens. Environ. 113, 62–72. https://doi.org/10.1016/j.rse.2008.08.012

Townsend, P.A., Serbin, S.P., Kruger, E.L., Gamon, J.A., 2013. Disentangling the contribution of biological and physical properties of leaves and canopies in imaging spectroscopy data. Proc. Natl. Acad. Sci. 110, E1074–E1074. https://doi.org/10.1073/pnas.1300952110

Ullah, S., Skidmore, A.K., Ramoelo, A., Groen, T.A., Naeem, M., Ali, A., 2014. Retrieval of leaf water content spanning the visible to thermal infrared spectra. ISPRS J. Photogramm. Remote Sens. 93, 56–64. https://doi.org/10.1016/j.isprsjprs.2014.04.005

Ustin, S.L., Gitelson, A.A., Jacquemoud, S., Schaepman, M., Asner, G.P., Gamon, J.A., Zarco-Tejada, P., 2009. Retrieval of foliar information about plant pigment systems from high resolution

spectroscopy. Remote Sens. Environ. 113, S67–S77. https://doi.org/10.1016/j.rse.2008.10.019

Vogelmann, J.E., Rock, B.N., Moss, D.M., 1993. Red edge spectral measurements from sugar maple leaves. Int. J. Remote Sens. https://doi.org/10.1080/01431169308953986

Waller, L.P., Allen, W.J., Barratt, B.I.P., Condron, L.M., França, F.M., Hunt, J.E., Koele, N., Orwin, K.H., Steel, G.S., Tylianakis, J.M., Wakelin, S.A., Dickie, I.A., 2020. Biotic interactions drive ecosystem responses to exotic plant invaders. Science (80-.). 368, 967–972. https://doi.org/10.1126/science.aba2225

Williams, L.J., Cavender-Bares, J., Townsend, P.A., Couture, J.J., Wang, Z., Stefanski, A., Messier, C., Reich, P.B., 2020. Remote spectral detection of biodiversity effects on forest biomass. Nat. Ecol. Evol. 5, 46–54. https://doi.org/10.1038/s41559-020-01329-4

Wilson, J.S., Lindsey, G.H., 2005. Socioeconomic correlates and environmental impacts of urban development in a central Indiana landscape. J. Urban Plan. Dev. https://doi.org/10.1061/(ASCE)0733-9488(2005)131:3(159)

Wolter, P.T., Mladenoff, D.J., Host, G.E., Crow, T.R., 1995. Improved forest classification in the northern Lake States using multi-temporal Landsat imagery. Photogramm. Eng. Remote Sensing 61, 1129–1143.

Yadeta, K.A., Thomma, Bart, P., 2013. The xylem as battleground for plant hosts and vascular wilt pathogens. Front. Plant Sci. 4, 1–12. https://doi.org/10.3389/fpls.2013.00097

Zarco-Tejada, P.J., Camino, C., Beck, P.S.A., Calderon, R., Hornero, A., Hernández-Clemente, R., Kattenborn, T., Montes-Borrego, M., Susca, L., Morelli, M., Gonzalez-Dugo, V., North, P.R.J., Landa, B.B., Boscia, D., Saponari, M., Navas-Cortes, J.A., 2018. Previsual symptoms of Xylella fastidiosa infection revealed in spectral plant-trait alterations. Nat. Plants 4, 432–439.

https://doi.org/10.1038/s41477-018-0189-7

Zarco-Tejada, P.J., González-Dugo, M.V., Fereres, E., 2016. Seasonal stability of chlorophyll fluorescence quantified from airborne hyperspectral imagery as an indicator of net photosynthesis in the context of precision agriculture. Remote Sens. Environ. 179, 89–103. https://doi.org/10.1016/j.rse.2016.03.024

Zarco-Tejada, P.J., Miller, J.R., Mohammed, G.H., Noland, T.L., Sampson, P.H., 2002. Vegetation Stress Detection through Chlorophyll a + b Estimation and Fluorescence Effects on Hyperspectral Imagery . J. Environ. Qual. https://doi.org/10.2134/jeq2002.1433